Marine and Petroleum Geology 98 (2018) 675–686

Contents lists available at ScienceDirect

Marine and Petroleum Geology

journal homepage: www.elsevier.com/locate/marpetgeo

Research paper

Reservoir characterization and hydrocarbon accumulation in late Cenozoic lacustrine mixed carbonate-siliciclastic fine-grained deposits of the northwestern Qaidam basin, NW China

Wei Zhang[a], Xing Jian[a,*], Ling Fu[b], Fan Feng[c], Ping Guan[d]

[a] State Key Laboratory of Marine Environmental Science, College of Ocean and Earth Sciences, Xiamen University, Xiamen 361102, PR China
[b] Research Institute of Petroleum Exploration and Development (RIPED), PetroChina, Beijing, 100083, PR China
[c] Petroleum Exploration and Production Research Institute, Sinopec, Beijing, 100083, PR China
[d] MOE Key Laboratory of Orogenic Belts and Crustal Evolution, School of Earth and Space Sciences, Peking University, Beijing, 100871, PR China

ARTICLE INFO

Keywords:
Reservoir
Hydrocarbon accumulation
Biomarker
Mixed carbonate-siliciclastic rock
Qaidam basin

ABSTRACT

Late Cenozoic lacustrine mixed carbonate-siliciclastic sequences in the northwestern Qaidam basin (NW China) are mainly composed of high porosity and low permeability fine-grained rocks but have big potentials of oil-gas commercial production. However, how these fine-grained rocks generate high-quality reservoirs and accumulate hydrocarbons, remains poorly known. This study focuses on shallow-buried Shang Youshashan Formation (Middle–Late Miocene, N_2^2) and Shizigou Formation (Late Miocene–Pliocene, N_2^3) reservoirs and hydrocarbons in Xiaoliangshan area of the northwestern Qaidam basin. We conduct mineralogy, petrography and porosity and permeability analysis for reservoir rocks and biomarker analysis for hydrocarbons and potential source rocks. The results indicate that the N_2^2 high-quality reservoirs are dominated by fractured marlstones and lime mudstones and constitute structural traps, whereas the N_2^3 hydrocarbon reservoirs are mainly composed of siliciclastic-dominantly rocks and form stratigraphic-lithologic traps. Similar biomarker ratios between crude oil samples and Paleogene organic matter-rich rocks reveal that hydrocarbons in the shallow system were likely derived from deep-buried source rocks, rather than late Cenozoic lacustrine fine-grained rocks themselves. In this case, large-scale vertical fractures created by kink band structures in the northwestern Qaidam basin are supposed to facilitate hydrocarbon migration and accumulation. Preliminary production data and exploration well oil-gas test results demonstrate highest yields and thus large hydrocarbon potentials in the N_2^2 marlstone and lime mudstone reservoirs. Collectively, we suggest that relatively high-permeability, fractured and carbonate-rich reservoirs on structural highs are favorable targets for future oil-gas exploration in the northwestern Qaidam basin. This petroleum system provides a typical and significant example for hydrocarbon exploration and development in mixed carbonate-siliciclastic fine-grained rocks of nonmarine petroliferous basins.

1. Introduction

It is widely realized that oil and natural gas production around the world have resulted in a decline of hydrocarbon reserves in conventional sandstone and carbonate rock reservoirs (Bentley, 2002). Unconventional reservoirs, such as tight sandstones, shales, mixed carbonate-siliciclastic fine-grained rocks and volcanic rocks, have received more and more attention (e.g. Pitman et al., 1982; Poppelreiter and Aigner, 2003; Delpino and Bermúdez, 2009; Clarkson et al., 2012; Zou et al., 2013; Macquaker et al., 2014). While mixed carbonate-siliciclastic sequences in marine environments and their implications for petroleum systems have been widely studied (e.g. Brooks et al., 2003; Coffey and Read, 2004; Barnaby and Ward, 2007; Garcia-Garcia et al., 2009; Lee and Chough, 2011; Zecchin and Catuneanu, 2017), investigation on formation mechanism of high-quality reservoirs in lacustrine mixed carbonate-siliciclastic fine-grained rocks and hydrocarbon accumulation processes, remains poorly reported.

Widespread Cenozoic lacustrine mixed carbonate-siliciclastic rocks have been discovered in the western Qaidam basin, northern Tibetan Plateau (Figs. 1 and 2; Hanson et al., 2001; Zhang et al., 2006; Song et al., 2010, 2014; Jian et al., 2014; Ji et al., 2017). Decades of hydrocarbon exploration by the Qinghai Oilfield Company, PetroChina demonstrate that those low-permeability mixed carbonate-siliciclastic fine-grained rocks don't only serve as high-quality hydrocarbon source

* Corresponding author.
E-mail address: xjian@xmu.edu.cn (X. Jian).

https://doi.org/10.1016/j.marpetgeo.2018.09.008
Received 12 June 2018; Received in revised form 4 September 2018; Accepted 7 September 2018
Available online 08 September 2018

rocks, but can also be high-potential oil and gas reservoirs (e.g. Hanson et al., 2001; He et al., 2008; Feng et al., 2013). Nanyishan and Jiandingshan oilfields, located in northwestern Qaidam basin (Fig. 1C), were successively found in the last century and have been exploited till now, where oil and gas are mainly stored in both deeply buried (ca. 2500–4000 m) Paleogene and shallow (ca. < 2500 m) Neogene mixed carbonate-siliciclastic sequences (Zhang et al., 2006; Feng et al., 2011; Wang et al., 2012). Previous reservoir characterization results indicate that formation of the deep hydrocarbon reservoirs is controlled by structural fracturing and diagenetic dissolution (Fu, 2010; Feng et al., 2011, 2013; Zeng et al., 2012), whereas reservoir space of the shallow sequences is dominated by primary pores in the mixed carbonate-siliciclastic rocks (Tang et al., 2013). Previous drilling and structural interpretation indicates that the Xiaoliangshan area (Fig. 1C) is located in a topographic depression and preserves a deeply-buried, organic matter-rich, fine-grained Cenozoic sedimentary succession (e.g. Jiang et al., 2009). Hence, the Xiaoliangshan area had been always considered as a significant hydrocarbon source region in the northwestern Qaidam petroleum system for a long time (Huang et al., 1989; Zhu et al., 2005; He et al., 2008; Jiang et al., 2009).

Recent exploration results (six exploration wells since 2010, Fig. 1D) of the Xiaoliangshan area indicate high potentials of commercial production for low-permeability hydrocarbon reservoirs in the shallow (500–2000 m) Neogene mixed carbonate-siliciclastic sequences. Reservoir petrography and high-quality hydrocarbon reservoir formation mechanism remain enigmatic, which results in high challenges of hydrocarbon exploration and severely restricts long-term exploration deployment in this area. Furthermore, the source and accumulation mechanism of the shallow-preserved oil resources in the Xiaoliangshan area remain open questions. These issues need to be solved to have a better understanding of the Xiaoliangshan petroleum system and to facilitate hydrocarbon exploration and production in the Qaidam basin.

In this study, we focus on the middle Miocene to Pliocene lacustrine mixed carbonate-siliciclastic sequences in the Xiaoliangshan area, northwestern Qaidam basin (Fig. 1), and mainly present results of mineralogy, petrography and petrophysical property analysis of reservoirs, biomarkers of crude oil and potential source rocks and some related production data. We attempt to answer: 1) what controls the development of high-quality hydrocarbon reservoir and 2) why and how hydrocarbons accumulated in the shallow mixed carbonate-siliciclastic sequences in the northwestern Qaidam basin.

2. Geological setting

The Qaidam basin is a nonmarine, petroliferous basin that lies in the northeastern corner of the Tibetan Plateau (Fig. 1). The basin floor sits about 2.7–3 km above sea level, and the basin is surrounded by three large mountain ranges that reach elevations of up to 5 km. To the south are the East Kunlun Mountains which separate the Qaidam basin from the Hoh Xil basin (Fig. 1). The Qilian Mountains are to the east as a ca. 300 km wide fold-thrust belt (Yin and Harrison, 2000). To the northwest are Altun Mountains, which are created by an active left-lateral strike-slip fault (Altyn Tagh Fault) and separate the Qaidam basin from the Tarim basin (Fig. 1).

The Qaidam basin contains an exceptionally thick Mesozoic and Cenozoic sedimentary succession of 3–16 km, which was mainly deposited in a fluvial-lacustrine depositional environment (Xia et al., 2001; Zhuang et al., 2011; Guan and Jian, 2013). Lower and Middle Jurassic are characterized by gray coal-bearing siliciclastic deposits, while Upper Jurassic and Lower Cretaceous strata mainly consist of red sand-dominant deposits (Cao et al., 2008, 2012; Jian et al., 2013a, 2018). It is well known that the depocenter of the basin shifted eastward during the Cenozoic (Wang et al., 2006; Yin et al., 2008; Bao et al., 2017). Hence, Cenozoic strata in the basin display spatial and temporal variations and mixed carbonate-siliciclastic deposits (e.g. Fig. 2) are mainly distributed in the western Qaidam basin (Song et al., 2010; Guan and Jian, 2013; Jian et al., 2013a; b; 2014; Ji et al., 2017). The Cenozoic strata can be divided into 7 stratigraphic units (Fig. 3) as follows: 1) Lulehe Formation (E_{1+2}, ~53.5–~45 Ma); 2) Xia Ganchaigou Formation (E_3, divided into E_3^1 and E_3^2 in the local hydrocarbon exploration and development, ~45–~35.5 Ma); 3) Shang Ganchaigou Formation (N_1, ~35.5–~22 Ma); 4) Xia Youshashan Formation (N_2^1, ~22–~15 Ma); 5) Shang Youshashan Formation (N_2^2, ~15–~8 Ma); 6) Shizigou Formation (N_2^3, ~8–2.8 Ma); and 7) Qigequan Formation ($Q_{1\text{-}2}$, 2.8 Ma–present).

The Qaidam basin is an important sedimentary basin for hydrocarbon exploration and production in northwest China, with the annual production at seven million tons oil equivalent since 2011 (Wang et al., 2012; Feng et al., 2013; Fu et al., 2016). The basin is usually divided into three major exploration & production areas, i.e., north margin block belt, west depression and sanhu depression (Fig. 1B), focusing on Jurassic–Paleogene, Paleogene–Neogene and Quaternary strata, respectively (e.g. Pang et al., 2004, 2005; Cao et al., 2008; Feng et al., 2013; Wang et al., 2015; Yu et al., 2016). Most natural gas is extracted from the east part of the basin, while crude oil is mainly collected from the western basin (Fig. 1B; Fu et al., 2016). The Nanyishan and Jiandingshan oilfields contribute most hydrocarbon production in the northwestern Qaidam basin over the past decades (Zhang et al., 2006; He et al., 2008; Feng et al., 2011; Wang et al., 2012). The Xiaoliangshan oilfield was recently found and the hydrocarbon resource has been mainly exploited from shallow-buried N_2^2 and N_2^3 carbonate-siliciclastic sequences (Wang et al., 2012).

3. Materials and methods

Wells L3 and L4 were first drilled by Qinghai Oilfield Company, PetroChina in 1981 and 1998, respectively. Exploration wells L101, L102, L103, L104, L5 and L6 (Fig. 1D) were drilled in 2010–2011, concentrating on shallow N_2^2 and N_2^3 sedimentary strata (Fig. 4). Rock cutting examination and conventional well logging (e.g. natural gamma-ray, spontaneous potential and acoustic logging) were conducted along with the drilling.

More than 400 m cores (e.g. Fig. 2) were obtained from the hydrocarbon exploration wells (e.g., L101 and L6). More than 1200 sedimentary rock samples were collected from these rock cores, and five crude oil samples were collected from Well L5 and two production wells (i.e., Wells 13–23 and 13–21). Sedimentary rock samples were made to regular and casting thin sections for petrography study. Alizarin red solution was used on the thin sections to distinguish carbonate minerals.

Porosity and permeability measurement was performed at Research Institute of Petroleum Exploration & Development of Qinghai Oilfield Company, PetroChina. A helium porosimeter was employed to obtain porosity (%) and density data for the samples. The permeability ($10^{-3} \times \mu m^2$, mD) was measured using a soap-film flowmeter at room temperature.

X-ray diffraction (XRD) analysis of rock powders was carried out on a Rigaku D/max-rA rotating anode X-ray diffractometer (12 KW). Each sample was continuously scanned under 40 kV, 100 mA, wave length of 1.5406, 2θ range of 3°–75°, step width of 0.02° and scanning speed of 4°/min.

Five rock samples (3 samples from N_2^2 strata and 2 samples from N_2^3 strata) and five crude oil samples (3 samples from N_2^2 reservoirs of exploration well L5 and 2 samples were collected from N_2^3 reservoirs of production wells) were selected for biomarker analysis. The rock samples were first crushed and then powdered to 100–200 mesh. The Soxhlet extraction approach (De Castro and Priego-Capote, 2010) was employed for organic matter separation. Detailed pretreatment and extraction procedures were given in Duan et al. (2006). Soluble organic matters were extracted twice using ultrasonication with a mixture of dichloromethane and methanol (2:1, v/v) for 56 h. Total hydrocarbons

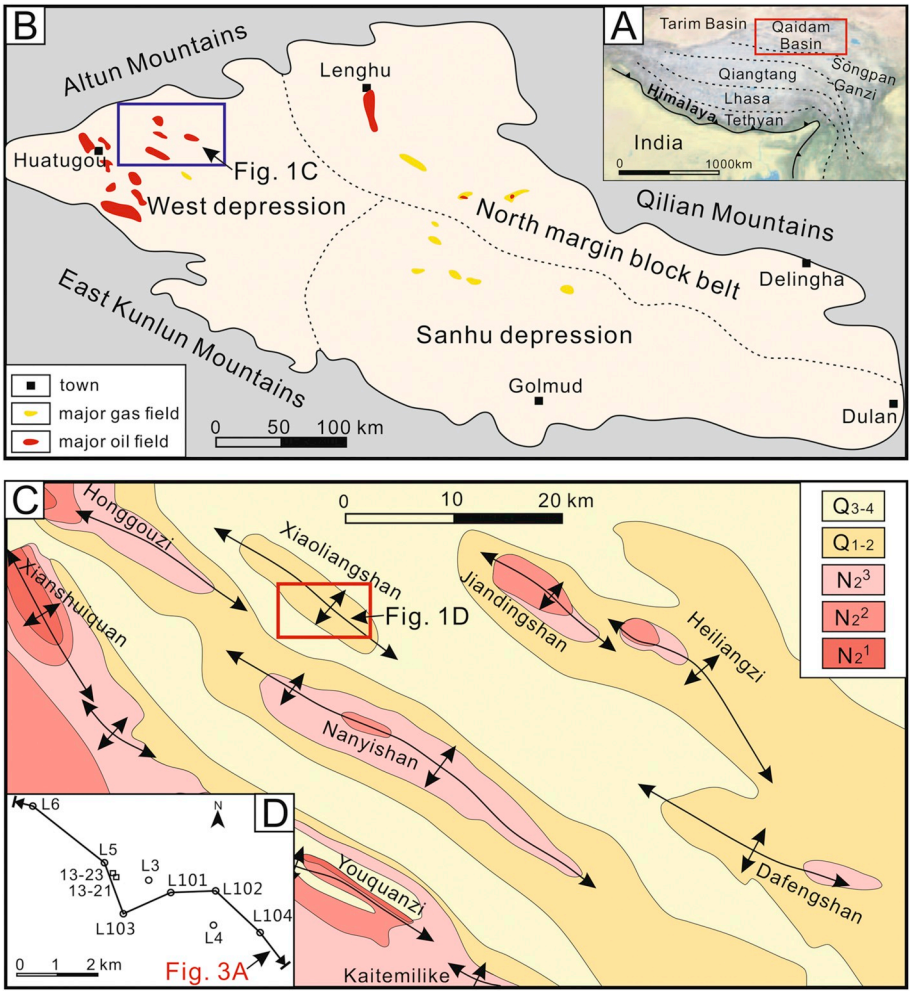

Fig. 1. (A) Location of the Qaidam basin. (B) Hydrocarbon production backgrounds of the Qaidam basin. (C) Geological map of the northwestern basin. (D) Major exploration wells (circles) in the Xiaoliangshan area (two crude oil samples were collected from production wells 13–23 and 13–21). N_2^1: Xia Youshashan Formation; N_2^2: Shang Youshashan Formation; N_2^3: Shizigou Formation; $Q_{1\text{-}2}$: Qigequan Formation; $Q_{3\text{-}4}$: Holocene.

were then eluted with n-hexane and saturated hydrocarbon components were separated from the extracts by column chromatography on alumina over silica gel. Those targeted organic matters were analyzed using an Agilent gas chromatography-mass spectrometry (GC6890N/MSD5973N). The detailed analytical procedures followed Duan et al. (2006) and Luo et al. (2016). The operating conditions in this study were: temperature ramped from 80 °C to 290 °C at 3 °C/min and held at 290 °C for 30 min, with He as carrier gas, and the ionization energy of the mass spectrometer was set to 70 eV.

4. Results

4.1. Stratigraphy correlation and oil-gas test of exploration wells

Based on cutting logging, well logging and 3-D seismic data, the subsurface N_2^2 and N_2^3 strata in the Xiaoliangshan area were correlated (Fig. 4). The upper part of N_2^2 strata drilled by those shallow exploration wells (L101, L102, L103, L104, L5 and L6) can be divided into Sequences S1, S2 and S3, and the N_2^3 strata can be separated into Sequences S4, S5 and S6. Oil-gas test (24 layers in total) of the exploration wells was conducted by the Qinghai Oilfield Company, PetroChina. Most of the test layers are located in Sequences S1 and S4 (Fig. 4A; Table A1 in Appendix A). Several oil-water layers appear in the Sequence S1 of Wells L101 and L5, whereas all the test layers in the Sequence S1 of Wells L102, L103, L104 and L6 are identified as water layers. Two test layers in Sequence S4 of Well L101 are oil layers, while the test layers in the same sequence of Well L103 are present as oil-water layers (Fig. 4A). Furthermore, these two oil-water layers of Well L103 have much larger average daily production (oil-gas test) than the two oil layers of Well L101 (Fig. 4A; Table A1).

4.2. Mineralogy

Typical XRD patterns and mineral composition results are shown in Fig. A1 (in Appendix A) and Table A2 (in Appendix A), respectively. Overall, the N_2^2 and N_2^3 sedimentary rocks have variable mineral compositions, and carbonate minerals (calcite and dolomite, with subordinate aragonite, siderite and magnesite) are abundant in the analyzed samples (Table A2). Several N_2^2 samples have greater than 60% carbonate mineral contents (Fig. 5A). Evaporite minerals (mainly including anhydrite and halite) are also very common in the sample, although most samples have less than 10% evaporite mineral contents (Fig. 5B). Samples with relatively high evaporite mineral contents (> 10%) dominantly distribute in the N_2^3 strata (Fig. 5B).

Fig. 5C–D displays the mineral compositions of three oil-gas test layers of Well L101. The results indicate that the N_2^2 hydrocarbon reservoir rocks have much higher carbonate contents and relatively lower evaporite mineral contents than the N_2^3 hydrocarbon reservoir rocks (Fig. 5C and D).

Fig. 2. Representative rock cores (A) and the corresponding lithology column (B) of Well L101 in the Xiaoliangshan area. The lithology column is based on on-site core description. The illustrated rock cores, which are mainly composed of marlstones and mudstones, were collected from 1347.09 m to 1359.19 m (N_2^2). The marlstones are characterized by macro-fractures (marked by yellow arrows) and show black and dark grey in colors, while the mudstones are characterized by abundant horizontal millimeter-scale laminations and show grey in colors. (For interpretation of the references to color in this figure legend, the reader is referred to the Web version of this article.)

4.3. Petrography

A variety of rock types were identified from the analyzed samples, including mudstone, lime mudstone, muddy siltstone, limy siltstone, siltstone, sandstone (dominated by lithic arenite and lithic wacke), marlstone, algal limestone and oolitic limestone. The sandstones are dominantly fine-grained and poorly to moderately sorted (Fig. 6A and B). Hydrocarbon reservoir rocks in the N_2^3 strata are mainly composed of immature muddy siltstones, siltstones and fine sandstones. These sedimentary rocks are weakly lithogenetic and are characterized by syn-depositional anhydrite minerals (Fig. 6A and B). Intergranular pore (primary) is the dominating reservoir space type in these siliciclastic-dominantly rocks (Fig. 6C). However, the hydrocarbon reservoir rocks in the N_2^2 strata are dominated by marlstones and lime mudstones, and post-depositional fractures dominate the reservoir space (Fig. 6D and E). It is worth noting that macro-fractures are also abundant in these carbonate-rich rocks (Fig. 2A). Furthermore, a 10 cm oolitic limestone layer with high porosity (primary intergranular pores) was recognized in the oil-gas test layer (1343–1357 m) of Well L101 (Fig. 6F).

4.4. Reservoir petrophysical properties

Overall, the N_2^2 and N_2^3 mixed carbonate-siliciclastic sequences of Well L101 are composed of high-porosity (most > 10%) and low-permeability (most < 50 mD) sedimentary rocks (Table A3 in Appendix A). The shallow-buried N_2^3 samples have overwhelmingly higher porosity values (averaging 28.5% for N_2^3, 21.8% for N_2^2) and similar ranges of permeability values (0.04–44 mD for N_2^3, averaging 3.8 mD; 0.03–60 mD for N_2^2, averaging 3.6 mD) than N_2^2 samples (Fig. 7A). Although the analyzed reservoir rocks with different oil-gas-bearing possibility (based on rock cutting logging data) do not show obvious difference on porosity and permeability values (Fig. 7B), samples from the N_2^2 oil-gas test layer of Well L101 have low porosity values (averaging 21.1%) and more variable permeability values (0.1–27 mD) (Fig. 7C). Samples from those two N_2^3 oil-gas test layer have relatively high porosity values (averaging 27.2%) and a much narrow range (0.4–9 mD, except a 33 mD value for a fine sandstone sample) of permeability values (Fig. 7C).

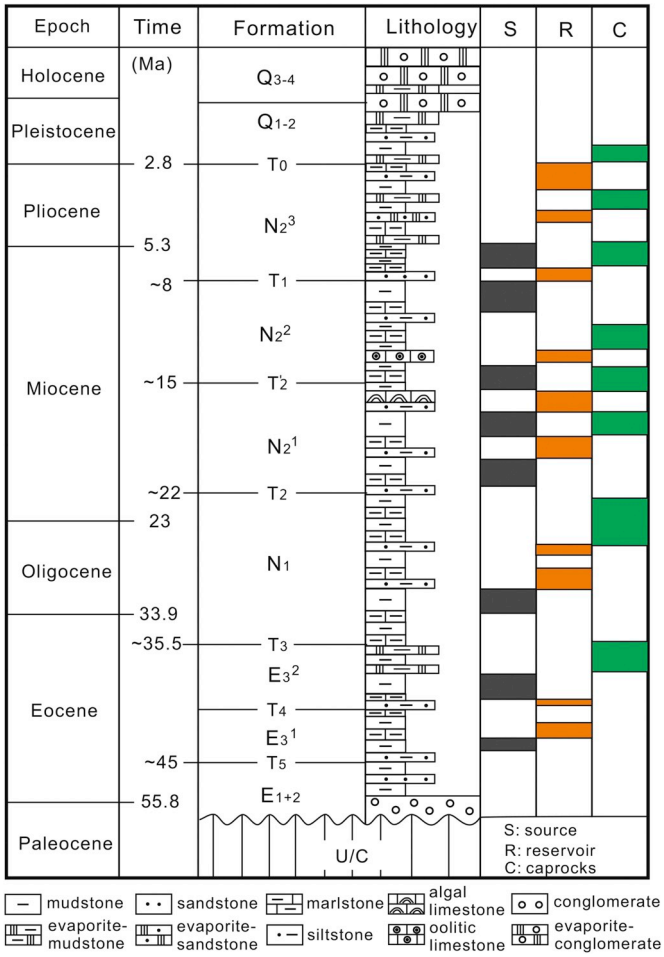

Fig. 3. Cenozoic stratigraphic framework, seismic reflectors, representative lithological column and source-reservoir-caprock patterns of the northwestern Qaidam basin, modified from Jian et al. (2013b) and Tang et al. (2013).

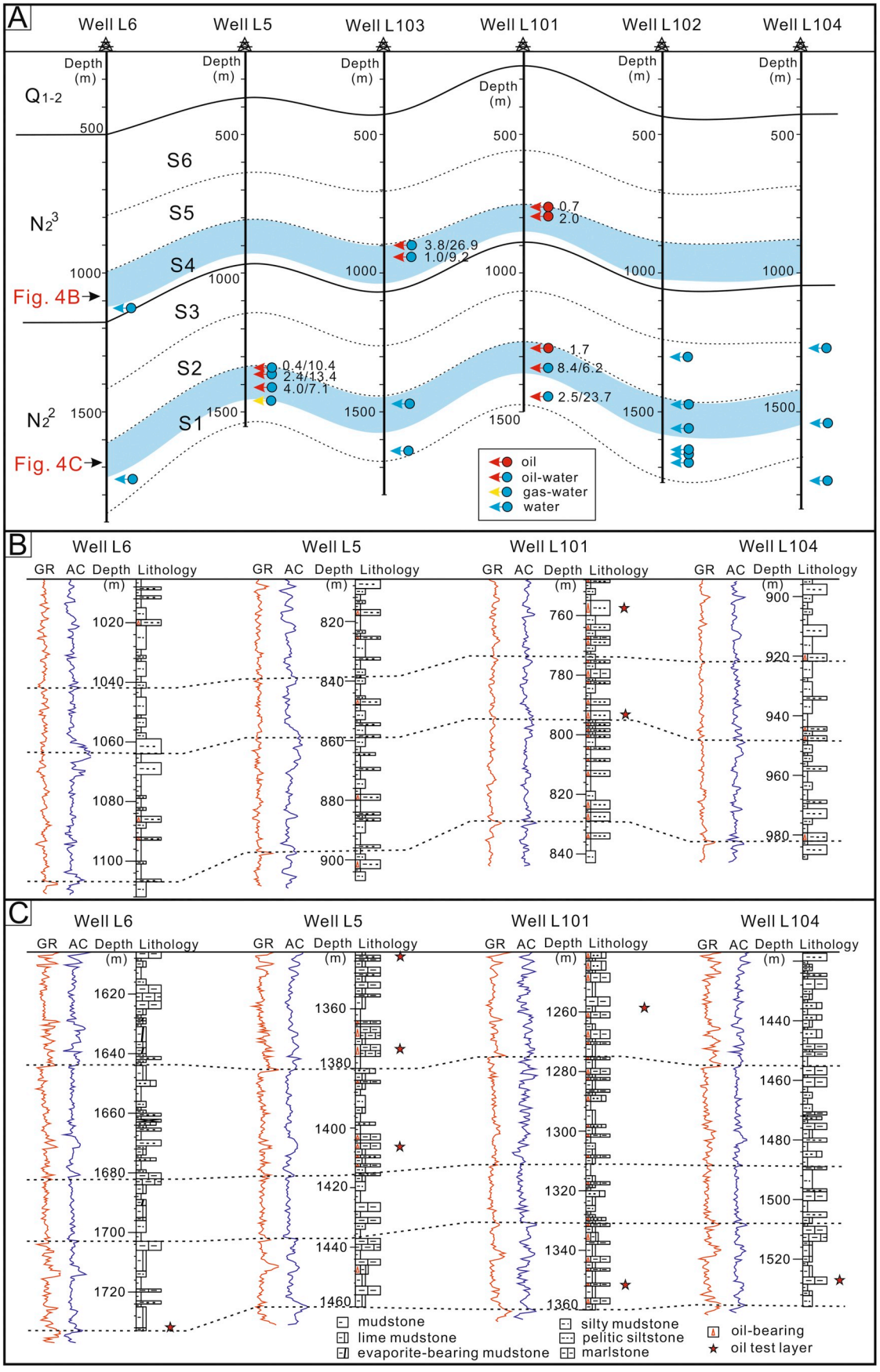

(caption on next page)

Fig. 4. (A) Subsurface stratigraphy framework and oil-gas test results of major drilling wells in the Xiaoliangshan area. The number close to the test layer symbol is the average daily production of oil/water. For data, see Table A1 in Appendix A. (B) and (C) Detailed stratigraphic correlation of the S4 and S1 sequences in the N_2^3 and N_2^2 sedimentary strata, respectively (blue bands in Fig. 4A). The black dash lines represent boundaries of sub-layers in a sequence. Lithologic logging and oil-bearing records are based on the rock cutting examination during the drilling. GR: natural gamma-ray logging; AC: acoustic logging. (For interpretation of the references to color in this figure legend, the reader is referred to the Web version of this article.)

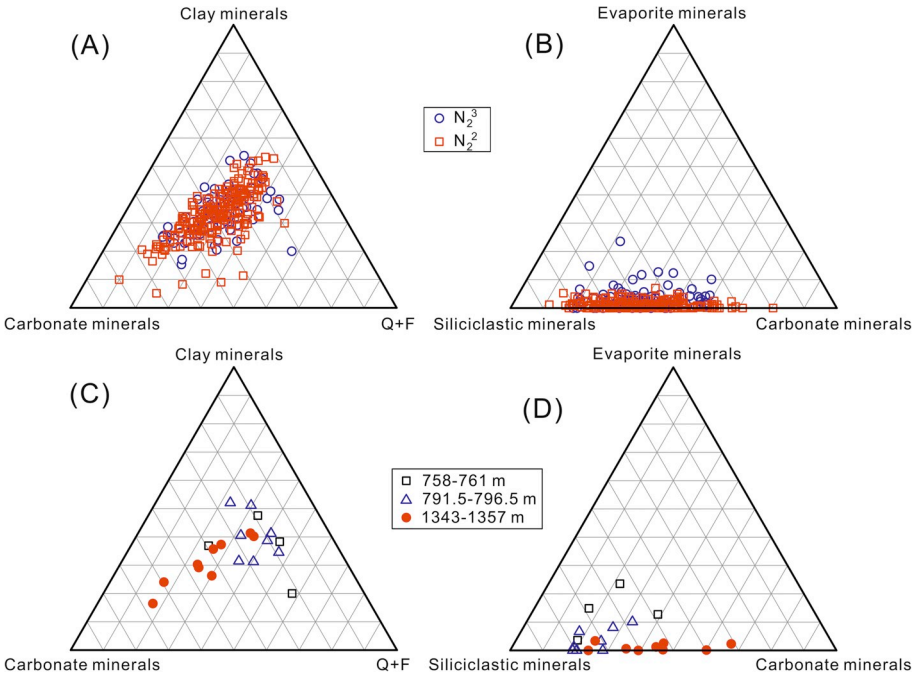

Fig. 5. XRD analysis-based mineral compositions of the N_2^2 and N_2^3 mixed carbonate-siliciclastic rocks in the Xiaoliangshan area (samples from Wells L101 and L6). (A) and (B): data of all the analyzed samples; (C) and (D): data of samples from three oil-test layers (1343–1357 m in N_2^2, 791.5–796.5 m and 758–761 m in N_2^3) of Well L101. For data, see Table A2 in Appendix A. Q + F: quartz, K-feldspar and plagioclase; Carbonate minerals: calcite, dolomite, aragonite, siderite and magnesite; Siliciclastic minerals: quartz, K-feldspar, plagioclase and clay minerals; Evaporite minerals: gypsum, anhydrite and halite.

4.5. Biomarker analysis

Several biomarkers, including n-alkanes, isoprenoid alkanes, terpanes and steranes, were employed to evaluate organic matter features of the rock and crude oil samples. Representative biomarker spectra are shown in Fig. A2 in Appendix B. The biomarker analysis results are shown in Table 1 and Fig. 8. The isoprenoid Pr/Ph and terpane Gammacerane/C_{30} hopane ratios are common biomarker parameters for depositional environments of hydrocarbon source rocks (e.g., Moldowan et al., 1986; Hughes et al., 1995; Luo et al., 2017, 2018a; b). The $\Sigma C_{22-}/\Sigma C_{23+}$ n-alkanes and sterane ααα-20R-C_{27}/C_{29} ratios are usually employed to evaluate organic matter types of the rocks (e.g., Seifert, 1978; Philp and Gilbert, 1986; Meyers and Ishiwatari, 1993). And the hopanoid C_{31}αβ-22S/22(S + R), steroid C_{29}-ααα-20S/20(S + R) and steroid C_{29}-ββ/(αα+ββ) ratios are frequently-used biomarker maturity parameters (e.g., van Graas, 1990; Farrimond et al., 1998; Luo et al., 2018a).

4.5.1. Biomarkers of sedimentary rock samples

The n-alkanes of the analyzed N_2^2 and N_2^3 sedimentary rocks distribute from C_{14} to C_{35} and are dominated by C_{16} or C_{22} homologues (Fig. A2). The $\Sigma C_{22-}/\Sigma C_{23+}$ values, which indicate dominance of short chain n-alkanes, range from 0.96 to 1.91 (Table 1; Fig. 8). These samples have OEP_1 (odd-even predominance of short chain n-alkanes) and OEP_2 (odd-even predominance of long chain n-alkanes) values ranging from 0.92 to 1.06 and from 1.00 to 1.41 (Table 1), respectively. Isoprenoid alkanes of the analyzed rock samples are dominated by phytane, and the N_2^3 samples have relatively higher Pr/Ph values than N_2^2

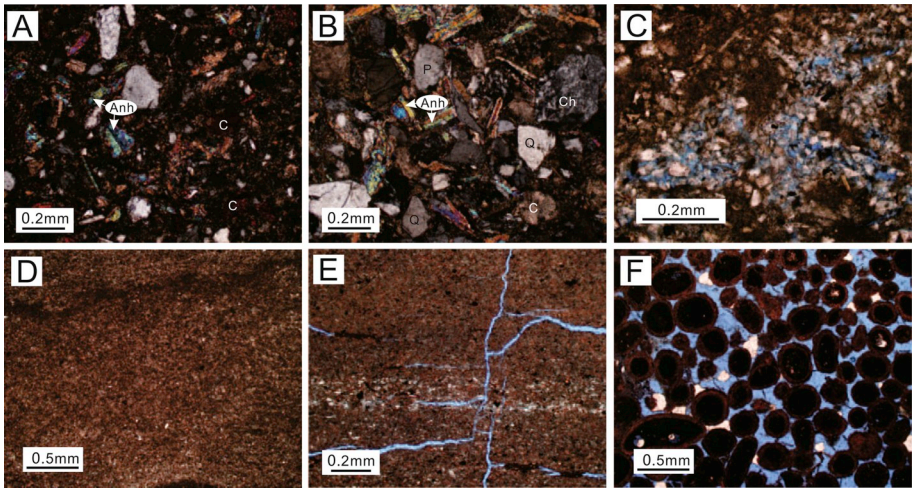

Fig. 6. Representative photomicrographs of hydrocarbon reservoir rocks of Well L101. (A) Immature and matrix-supported siltstone (758.6 m); (B) fine sandstone with abundant anhydrite matrixes (792.6 m); (C) intergranular pores (blue) in the siltstone reservoir (758.0 m). (D) Marlstone (1348.2 m). (E) Microfractures (blue) in the marlstone reservoir. (F) Oolitic limestone and intergranular pores (primary) (1355.8 m). Anh: anhydrite; Q: quartz; P: plagioclase; C: carbonate; Ch: chert. (For interpretation of the references to color in this figure legend, the reader is referred to the Web version of this article.)

samples, with ranges of 0.58–0.62 and 0.26–0.38 (Table 1; Fig. 8), respectively. Terpanes of the samples are dominated by pentacyclic triterpenes, and the Gammacerane/C_{30} hopane ratios range from 0.17 to 0.53 (Table 1). Steranes of the samples are characterized by high ααα-20R cholestanes, medium ααα-20S cholestanes as well as low αββ cholestanes and diacholestanes. The ST-C_{29}-ααα-20S/20(S + R), ST-C_{29}-ββ/(αα+ββ) and ST-ααα-20R-C_{27}/C_{29} ratios have ranges of 0.05–0.41, 0.23–0.39 and 0.48–1.24 (Table 1), respectively.

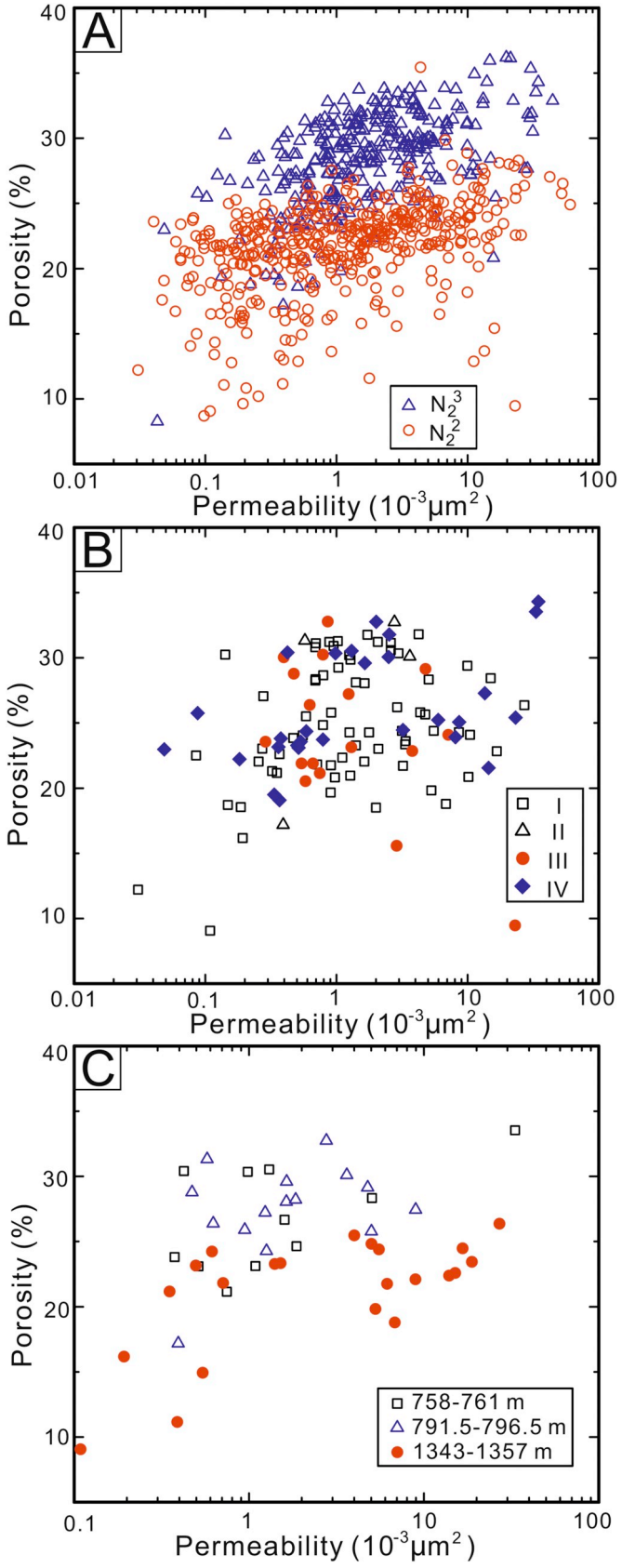

Fig. 7. Binary plots of permeability vs. porosity. (A) Porosity and permeability data of all the samples from Well L101. (B) Porosity and permeability data of oil-gas-bearing reservoir samples from Well L101. In this study, the oil-gas-bearing possibility was determined during rock cutting examination and can be classified into 4 levels: I (fluorescent, cannot be seen by naked eyes), II (oil stained, the oil-bearing part taking < 5% of the sample), III (oil patch, 5–30%) and IV (oil immersed, 30–60%). (C) Comparison of the porosity and permeability data of samples from three oil-test layers of Well L101. For data, see Table A3 in Appendix A.

4.5.2. Biomarkers of crude oil samples

Overall, the crude oil samples from N_2^2 and N_2^3 reservoirs have similar biomarker compositions. $\Sigma C_{22-}/\Sigma C_{23+}$ ratio, OEP_1 and OEP_2 values of n-alkanes for the crude oil samples have ranges of 0.98–1.32, 0.78–1.14 and 0.94–1.00, respectively (Table 1). Pr/Ph and Gammacerane/C_{30} hopane values display small ranges of 0.35–0.39 and 0.50–0.61, respectively. Furthermore, N_2^2 and N_2^3 crude oil samples have relatively consistent sterane compositions and thus show small ranges of ST-C_{29}-ααα-20S/20(S + R), ST-C_{29}-ββ/(αα+ββ) and ST-ααα-20R-C_{27}/C_{29} ratios (Table 1; Fig. 8), varying from 0.34 to 0.41, from 0.34 to 0.39 and from 0.98 to 1.07, respectively.

5. Interpretation and discussion

5.1. Formation of shallow-buried hydrocarbon reservoirs

Both XRD analysis-based mineralogy and petrography results indicate that the subsurface N_2^2 and N_2^3 sedimentary strata in the Xiaoliangshan area mainly consist of mixed carbonate-siliciclastic rocks (Figs. 5 and 6). This is consistent with on-site core description and rock cutting logging data (e.g. Figs. 2 and 4). Previous sedimentary facies analysis suggests that these fine-grained rocks were deposited in lake environments under relatively arid climate conditions, and the lake water became increasingly shallow and brackish over time (from a semi-deep fresh to semi-brackish lake environment to a shallow brackish lake environment) during the middle–late Miocene (Jian et al., 2014). The arid climates and salinization of lake water are also supported by abundant syn-depositional evaporite minerals in the N_2^3 sedimentary rock samples (Fig. 5B) and relatively high Gammacerane/C_{30} hopane values of the analyzed samples (Table 1). High Gammacerane in sediments has been commonly considered to be associated with highly stratified and saline water columns (Fu et al., 1992; Damsté et al., 1995; Stephens and Carroll, 1999).

It is well acceptable that the northwestern Qaidam basin was regionally in underwater environments with low input of clastic detritus (or away from drainages) during the Miocene to Pliocene (e.g. Zhang et al., 2006; Tang et al., 2013; Jian et al., 2014; Ji et al., 2017). This kind of sedimentary environment couldn't generate thick and widely-extended siliciclastic rock sequences. This results in high challenges of seeking high-quality reservoir and thus hydrocarbon exploration in this area. Petrographic results demonstrate that primary intergranular pore in muddy siltstones, siltstones and fine sandstones dominates the reservoir space in the N_2^3 strata, whereas micro-fractures in marlstones and lime mudstones of the N_2^2 strata are an important reservoir space type (Fig. 6). The generally low and variable permeability values of the samples from the N_2^2 oil-test layer (i.e. 1343–1357 m) of Well L101 (Fig. 7C) imply that the micro-fractures are probably heterogeneously distributed in carbonate-rich rocks. Besides, macro-fractures (Fig. 2A) probably serve as a significant role on the formation of high-quality reservoirs in the N_2^2 strata. Although those N_2^3 siliciclastic-dominantly

Table 1
Organic geochemical indicators of source rock and crude oil samples in the Xiaoliangshan area, northwestern Qaidam basin.

Sample information and biomarker proxy		Rock samples					Crude oil samples				
		L101-5	L101-10	L101-25	L101-28	L101-35	XLS-1	XLS-2	XLS-3	XLS-4	XLS-5
Sample information	Well	L101	L101	L101	L101	L101	L5	L5	L5	13–21	13–23
	Formation	N_2^2	N_2^2	N_2^2	N_2^3	N_2^3	N_2^2	N_2^2	N_2^2	N_2^3	N_2^3
	Depth (m)	1397.5	1379.52	1239.33	804.14	762.93	1467.5	1408	1374.3	759	760
N-alkanes	$\Sigma C_{22-}/\Sigma C_{23+}$ n-alkanes	0.96	1.45	1.59	1.26	1.91	1.27	1.32	1.06	1.09	0.98
	OEP_1	0.95	0.92	1.0	0.94	1.06	0.93	1.05	1.14	1.07	0.78
	OEP_2	1.00	1.02	1.04	1.41	1.06	0.99	0.99	1.00	1.04	0.94
Isoprenoids	Pr/Ph	0.38	0.33	0.26	0.58	0.62	0.38	0.39	0.38	0.35	0.36
Terpanes	Gammacerane/C_{30} hopane	0.53	0.29	0.42	0.17	0.36	0.51	0.61	0.50	0.50	0.58
	HOP-C_{31}αβ-22S/22(S + R)	0.60	0.56	0.75	0.58	0.60	0.62	0.56	0.60	0.62	0.61
Steranes	ST-C_{29}ααα-20S/20(S + R)	0.24	0.09	0.05	0.41	0.36	0.34	0.41	0.38	0.40	0.41
	ST-C_{29}-ββ/(αα + ββ)	0.33	0.23	0.25	0.36	0.39	0.38	0.39	0.37	0.34	0.37
	ST-ααα-20R-C_{27}/C_{29}	0.93	0.93	0.48	1.24	0.96	1.00	1.07	0.98	0.99	1.07

ST: steroid hydrocarbons; HOP: hopanoid hydrocarbons. $\Sigma C_{22-}/\Sigma C_{23+}$ n-alkanes: sum of C_{12} to C_{22}/sum of C_{23} to C_{38} n-alkanes; $OEP_1 = (C_{17}+6*C_{19}+C_{21})/(4*C_{18}+4*C_{20})$ n-alkanes; $OEP_2 = (C_{25}+6*C_{27}+C_{29})/(4*C_{26}+4*C_{28})$ n-alkanes; Pr/Ph: pristine/phytane; HOP-C_{31}αβ-22S/22(S + R): C_{31}-αβ-homohopanes 22S/22(S + R); ST-C_{29}-ααα-20S/20(S + R): C_{29}-ααα-24-ethyl-cholestanes 20S/20(S + R); ST-C_{29}-ββ/(αα + ββ): C_{29}-24-ethyl-cholestanes (αββ 20S + αββ 20R)/(ααα 20S + ααα 20R + αββ 20S + αββ 20R); ST-ααα-20R-C_{27}/C_{29}: ααα 20R cholestane/24-ethyl-cholestane.

rocks have higher porosity values than the N_2^2 carbonate-rich rocks (Fig. 7), given the limited distribution of the siliciclastic-dominantly rocks, we suggest that the best hydrocarbon reservoirs in the Xiaoliangshan area are located in the N_2^2 carbonate-rich and fractured sedimentary sequences. This conclusion is reinforced by the oil-gas test results (Fig. 4A; Table A1), which show that the Sequence S1 of the N_2^2 strata indicates high oil-water yields. Since the shallow-buried carbonate-siliciclastic rocks are of high porosity and low permeability (Figs. 6 and 7), permeability is the most important factor for formation of high-quality reservoirs. Therefore, unravelling the fracture distribution in the carbonate-siliciclastic fine-grained rocks is a key for hydrocarbon exploration and development in the shallow-buried strata of the Xiaoliangshan area.

The significance of fractures is also advocated by previous studies on Paleogene lacustrine carbonate reservoirs of the western Qaidam basin, which indicate that occurrence and abundance of open fractures mainly control the distribution of favorable reservoirs (Fu, 2010; Zeng et al., 2012 and reference therein). However, the shallow-buried Neogene reservoirs in this study have quite different reserving space types with the deep Paleogene reservoirs, where diagenetic dissolution also plays a major role on the formation of high-quality hydrocarbon reservoirs (Feng et al., 2011, 2013).

Furthermore, grainstone, such as oolitic limestone (e.g. Fig. 6F) and algal limestone sequences, are also regarded as significant targets for searching high-quality reservoirs in the northwestern Qaidam basin (Zhao, 2015). Another typical case of the grainstone as an important reservoir rock type in a lacustrine mixed carbonate-siliciclastic petroleum system is the Lower Triassic Rogenstein Member of the Buntsandstein Formation at De Wijk and Wanneperveen fields, NE Netherlands, where oolitic limestone beds have excellent reservoir petrophysical properties and serve as gas reservoirs, and overlying low-permeability claystones serve as cap rocks (Palermo et al., 2008).

5.2. Source of shallow-preserved hydrocarbons

Although total organic carbon (0.4%–1%) and chloroform bitumen "A" (as high as 0.35%) proxies reveal that the N_2^2 and N_2^3 sedimentary rocks in the Xiaoliangshan area have pretty high abundances of organic matters and thus can be high-quality source rocks of hydrocarbons, relatively low rock pyrolysis temperature T_{max} (360°C–420 °C) and vitrinite reflectance values (most < 0.6% (Fig. A3)) indicate that the shallow-buried fine-grained rocks are of low-maturity (He et al., 2008; Jiang et al., 2009; Wang et al., 2012). The low ST-C_{29}-ααα-20S/20(S + R) ratios (ranging from 0.05 to 0.24) for the analyzed N_2^2 rock samples (Table 1; Fig. 8) also support relatively low thermal maturity of the rocks (van Graas, 1990; Farrimond et al., 1998). Note that the N_2^3 rock samples have higher ST-C_{29}ααα-20S/20(S + R) and ST-C_{29}-ββ/(αα + ββ) values (with ranges of 0.36–0.41 and 0.36–0.39, respectively) than those N_2^2 rock samples (Table 1; Fig. 8), implying probable presence of intense biodegradation on the N_2^3 rocks. Previous studies suggest that biodegradation on organic matter-rich rocks can accelerate transformation from the biological configuration into the more stable geological configuration, and thus increases ST-C_{29}ααα-20S/20(S + R) and ST-C_{29}-ββ/(αα + ββ) values (e.g. Curry et al., 1994; Sun et al., 2009). This signifies that the thermal maturities of the shallow rocks are likely overestimated using these biomarker maturity parameters. By contrast, the crude oil samples from the N_2^2 and N_2^3 reservoirs have much higher ST-C_{29}ααα-20S/20(S + R) values (with the range of 0.34–0.41), revealing high maturity (Fig. 9) and have obviously different chromatograms with the N_2^2 and N_2^3 sedimentary rock samples (Fig. A2). Therefore, we conclude that the late Cenozoic (N_2^2 and N_2^3) lacustrine fine-grained rocks in the Xiaoliangshan area, i.e. the reservoir rocks themselves, are likely not source rocks for the shallow-preserved hydrocarbons.

Biomarker data of potential source rocks from the adjacent regions (including Jiandingshan, Hougouzi, Nanyishan, Dafengshan, Youquanzi and Kaitemilike areas) in the northwestern Qaidam basin and data of the deeply buried strata of Xiaoliangshan area were collected from Huang et al. (1989), Zhu et al. (2005), Zhao et al. (2007), He et al. (2008) and Lu et al. (2008) for the oil-source rock correlation (Fig. 9). Based on an integrated comparison of the various biomarker ratios, we conclude that the shallow-preserved hydrocarbons are most likely derived from E_3^2 and N_1 rocks in the Nanyishan area, or N_1 rocks of Xiaoliangshan and Dafengshan areas. This can be explained as follows. First, the N_2^2 and N_2^3 crude oil samples have obviously higher Gammacerane/C_{30} hopane (averaging in 0.54) and ST-C_{29}ααα-20S/20(S + R) (averaging in 0.39) values than most of the collected N_2^1 sedimentary rocks (Fig. 9). Thus, N_2^1 sedimentary rocks of the northwestern Qaidam basin are not sources rocks for the shallow-preserved hydrocarbons. The analyzed crude oil samples have similar values for most biomarker proxies with N_1 rocks in the northwestern basin, and the E_3^2 rocks in Nanyishan area, rather than other areas. For instance,

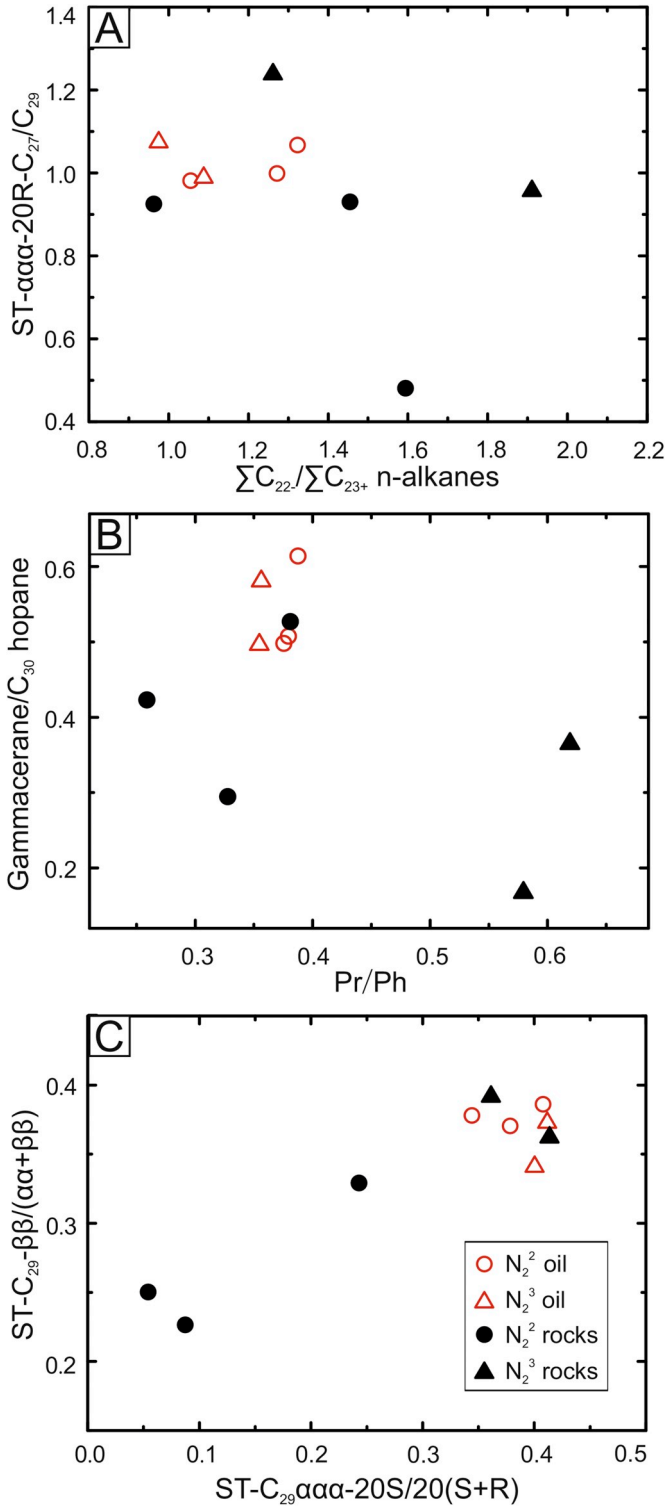

Fig. 8. Representative biomarker proxies of the analyzed rock and crude oil samples. Binary plots of (A) $\Sigma C_{22-}/\Sigma C_{23+}$ n-alkanes vs. ST-ααα-20R-C_{27}/C_{29}; (B) Pr/Ph vs. Gammacerane/C_{30} hopane; (C) ST-C_{29}-ααα-20S/20(S + R) vs. ST-C_{29}-ββ/(αα + ββ). For abbreviations and values of the biomarker ratios, refer to Table 1. Note that the biomarker-based maturity proxy values of the rock samples, such as ST-C_{29}-ααα-20S/20(S + R) and ST-C_{29}-ββ/(αα + ββ) values, are likely enhanced by biodegradation, based on relatively low Ro values (< 0.6%) of shallow-buried sedimentary rocks of the Xiaoliangshan area (Fig. A3 in Appendix A).

the ST-C_{29}-ββ/(αα + ββ) values of E_3^2 rocks in the Xiaoliangshan area are greater than 0.4; the $\Sigma C_{22-}/\Sigma C_{23+}$ n-alkanes of E_3^2 rocks in the Dafengshan area are greater than 1; and the ST-ααα-20R-C_{27}/C_{29} value of E_3^2 rocks in the Jiandingshan area is ca. 0.5. All these values are much higher or lower than the corresponding biomarker ratios of the

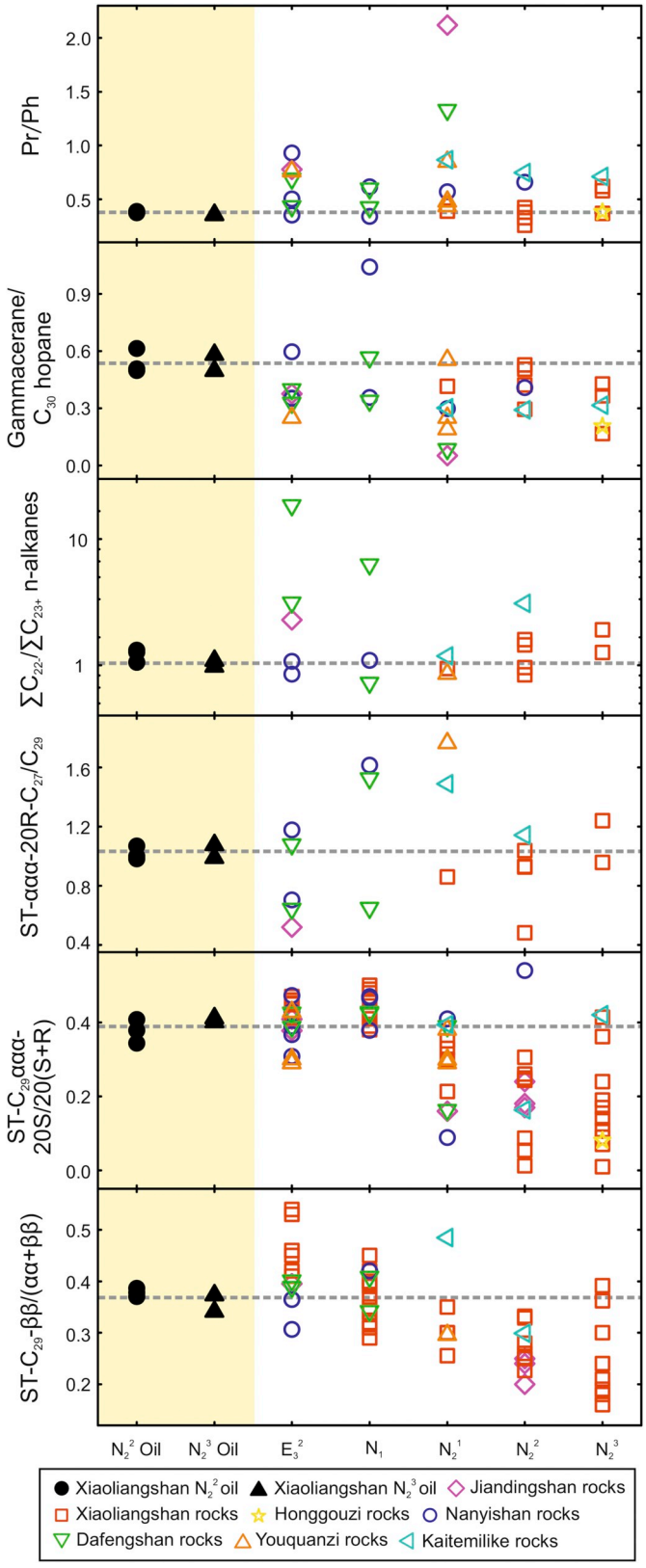

(caption on next page)

Fig. 9. Biomarker-based comparison of shallow-preserved hydrocarbons in Xiaoliangshan area and potential source rocks from the northwestern Qaidam basin. The horizontal dashed lines indicate averages of biomarker ratios of the analyzed crude oil samples. Note that hydrocarbons in the N_2^2 and N_2^3 strata of the Xiaoliangshan area are most likely from Paleogene source rocks, including E_3^2 rocks of Nanyishan area as well as N_1 rocks of Nanyishan, Xiaoliangshan and Dafengshan areas, specifically. Refer to Table 1 for the abbreviations of the biomarker proxies. The biomarker data in addition to the data in this study are from Huang et al. (1989), Zhu et al. (2005), Zhao et al. (2007), He et al. (2008) and Lu et al. (2008).

analyzed crude oil samples (Fig. 9). Note that a more rigorous hydrocarbon source could be concluded if there is a big published dataset for the Paleogene rocks in the northwestern Qaidam basin. Nevertheless, we contend the significance of Paleogene rocks in nearby regions for providing hydrocarbons to the shallow reservoirs of the Xiaoliangshan area.

5.3. Hydrocarbon accumulation in the late cenozoic lacustrine mixed carbonate-siliciclastic sequences

Given that the shallow-buried strata in this region are mainly composed of fine-grained lacustrine sedimentary rocks, any overlying mud-rich, or micritic carbonate-rich, low-permeability rocks can act as cap rocks for those hydrocarbon reservoirs. From the perspective of mineralogy and petrography, there is no obvious difference between reservoir rocks and cap rocks in the late Cenozoic lacustrine mixed carbonate-siliciclastic petroleum system (Figs. 5 and 6), except the minor siltstone, fine sandstone and oolitic limestone reservoirs (Fig. 6). This means that any post-depositional cracks or diagenetic infillings could lead to mutual conversion between cap and reservoir rocks.

The N_2^3 hydrocarbon traps are interpreted based on preliminary production data. About 40 shallow production wells were drilled in the anticlinal axis regions of the Xiaoliangshan area (Fig. 10), focusing on the upper part of Sequence S4 of the N_2^3 strata (Wang et al., 2012). Hydrocarbons were persistently exploited by the Qinghai Oilfield Company during 2010–2011. The results show that the production wells close to Well L103 have highest hydrocarbon and water yields, whereas those wells in the structural high have relatively low yields (Fig. 10). It is consistent with oil-gas test results of exploration wells L101 and L103, which demonstrate that the Sequence S4 of Well L103 has much larger hydrocarbon and water production, compared with Well L101 (Fig. 4A). Additionally, faults are not developed in the relatively high production region (Fig. 11). All these findings suggest that the siliciclastic-dominantly hydrocarbon traps in the N_2^3 strata are likely stratigraphic-lithologic traps, rather than structural traps. By contrast, the oil-gas test results reveal that the carbonate-rich reservoirs in the N_2^2 strata and corresponding hydrocarbon and water therein constitute typical structural traps (Fig. 4A). The test layers on the structural high indicate overwhelming oil and oil-water signals, while those layers in the relatively low region mainly indicate water signals (Fig. 4A).

Since the shallow oil resources in the Xiaoliangshan area were derived from deep-buried hydrocarbon source rocks, a large-scale vertical migration system is required for the hydrocarbon accumulation. Deformation and shortening of the Cenozoic sedimentary strata in the Qaidam basin is regarded as a result of the convergent setting between the India and Asia plates (e.g. Yin and Harrison, 2000; Wang et al., 2006; Zhou et al., 2006). Although the hydrocarbon-bearing structures within the Qaidam basin are mostly interpreted as high-angle thrust faults (e.g. Zhou et al., 2006; Bao et al., 2017), we favor the structures in northwestern Qaidam basin (e.g. Nanyishan, Jiandingshan and Xiaoliangshan structures) are featured by kink band-dominating anticlines (Mo et al., 2007; Zheng et al., 2007). Ideally, a kink band is a parallel-sided zone transecting foliation, within which the foliation is rotated by slip on itself (Faill, 1969; Suppe et al., 1997). Fold geometry of this kind of structure indicates that the anticlinal hinge-zones are cracked but connected (Fig. 11C). This is revealed by the NE-SW seismic profile of the Xiaoliangshan structure (Fig. 11A), which shows no obviously large-scale vertical faults deforming the N_2^2 and N_2^3 sedimentary strata. In this case, the conjugated kink bands can serve as a transport channel system for hydrocarbon migration (Fig. 12). Furthermore, the fractures created by kink bands in some cases can also be reservoir space for hydrocarbon accumulation (Mo et al., 2007).

6. Conclusions

This study conducts mineralogy, petrography, reservoir petrophysical property analysis and biomarker analysis of shallow-buried lacustrine mixed carbonate-siliciclastic fine-grained rocks from the Xiaoliangshan area of northwestern Qaidam basin, combines oil-gas test results of major exploration wells and preliminary production data, and yields the following conclusions about the complicated hydrocarbon system:

1) The hydrocarbons in the shallow N_2^2 and N_2^3 reservoirs of the Xiaoliangshan area are likely from deep-buried Paleogene source rocks (E_3^2 and N_1 in the Nanyishan area, or N_1 rocks in the Xiaoliangshan and Dafengshan areas, specifically), rather than the late Cenozoic lacustrine fine-grained rocks themselves. And large-scale vertical fractures created by kink band structures provide a potential migration system for the hydrocarbon accumulation.
2) The shallow hydrocarbon system in the Xiaoliangshan area at least has two hydrocarbon trap types. Structural traps and stratigraphic-lithologic traps dominate major hydrocarbon traps in the N_2^2 and N_2^3 strata, respectively.

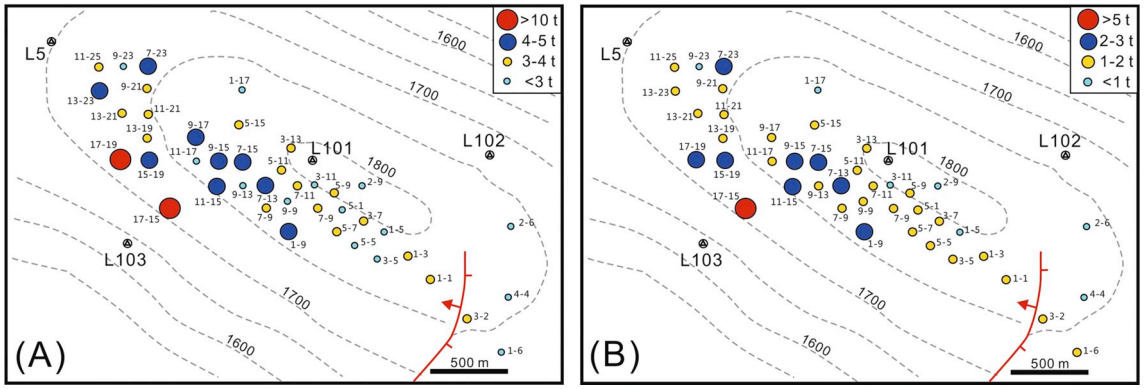

Fig. 10. Average daily production data (A: oil and water; B: oil, collected from 2010.08 to 2011.07 by pumping) of the N_2^3 oil layers of major production wells in the Xiaoliangshan oil field. Gray dashed lines are contour lines of the bottom of the N_2^3 strata.

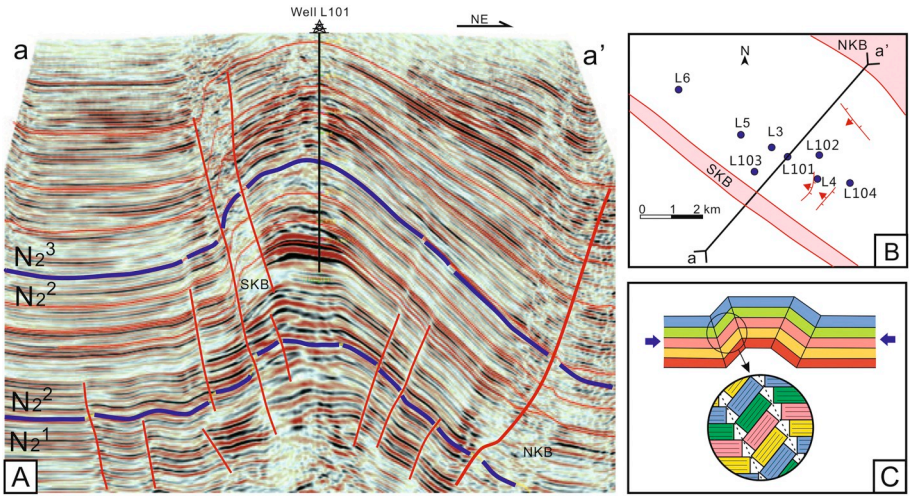

Fig. 11. Structural pattern of the Miocene strata in the Xiaoliangshan oil field. (A) Typical seismic section shows an anticline with kink band features; (B) Plane distribution of the two kink bands (red) and the major exploration wells; (C) Sketch of a kink band model and fractures therein. Note that the anticlinal hinge-zones are cracked but connected, which probably serve as a large-scale vertical migration system for hydrocarbon accumulation. (For interpretation of the references to color in this figure legend, the reader is referred to the Web version of this article.)

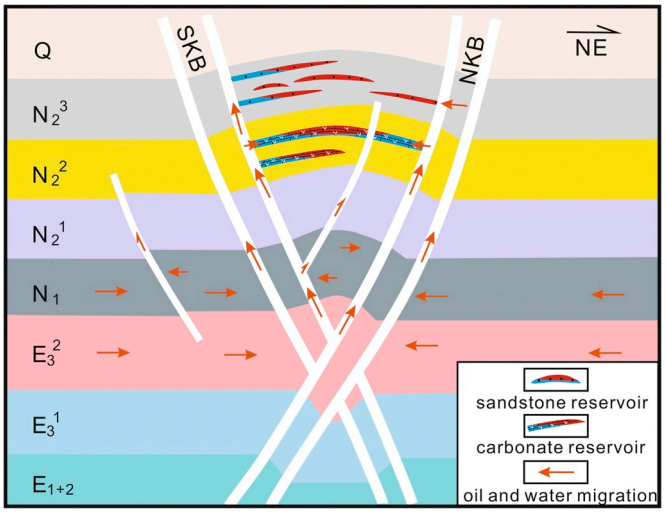

Fig. 12. Hydrocarbon accumulation model of the shallow-buried mixed carbonate-siliciclastic sequences in the Xiaoliangshan area, northwestern Qaidam basin.

3) High-quality reservoirs in the N_2^2 strata are dominated by fractured marlstones and lime mudstones, while siliciclastic-dominantly rocks serve as major hydrocarbon reservoir rock types in the N_2^3 strata.
4) As the mixed carbonate-siliciclastic fine-grained rocks are of high porosity and low permeability, we suggest that looking for relatively fractured, high-permeability and carbonate-rich reservoirs on structural highs in the northwestern Qaidam basin would be a primary direction for future oil-gas exploration.

Acknowledgments

This research was supported by the National Natural Science Foundation of China (No. 41806052), Natural Science Foundation of Fujian Province (No. 2017J05067), and Xiamen University Fundamental Research Funds for the Central Universities (No. 20720160114). Shibiao Deng, Jiawei Tang and Rui Zhang are thanked for their help during the sampling. We would like to thank Daowei Zhang, Yongshu Zhang, Jun Cui and Weiyong Zhao of Qinghai Oilfield Company for performing the porosity and permeability measurement and participating the study. We appreciate Qianxiang Meng of Key Laboratory of Petroleum Resources Research (Lanzhou), Institute of Geology and Geophysics, Chinese Academy of Sciences for his help during the biomarker analysis. Two anonymous reviewers provided constructive and thoughtful comments that improved this manuscript.

Appendix A. Supplementary data

Supplementary data related to this article can be found at https://doi.org/10.1016/j.marpetgeo.2018.09.008.

References

Bao, J., Wang, Y., Song, C., Feng, Y., Hu, C., Zhong, S., Yang, J., 2017. Cenozoic sediment flux in the Qaidam Basin, northern Tibetan Plateau, and implications with regional tectonics and climate. Global Planet. Change 155, 56–69.
Barnaby, R.J., Ward, W.B., 2007. Outcrop analog for mixed siliciclastic–carbonate ramp reservoirs—stratigraphic hierarchy, facies architecture, and geologic heterogeneity: grayburg Formation, Permian Basin, USA. J. Sediment. Res. 77, 34–58.
Bentley, R.W., 2002. Global oil & gas depletion: an overview. Energy Pol. 30, 189–205.
Brooks, G.R., Doyle, L.J., Suthard, B.C., Locker, S.D., Hine, A.C., 2003. Facies architecture of the mixed carbonate/siliciclastic inner continental shelf of west-central Florida: implications for Holocene barrier development. Mar. Geol. 200, 325–349.
Cao, J., Hu, K., Wang, K., Bian, L., Liu, Y., Yang, S., Wang, L., Chen, Y., 2008. Possible origin of 25-norhopanes in Jurassic organic-poor mudstones from the northern Qaidam Basin (NW China). Org. Geochem. 39, 1058–1065.
Cao, J., Wu, M., Chen, Y., Hu, K., Bian, L., Wang, L., Zhang, Y., 2012. Trace and rare earth element geochemistry of Jurassic mudstones in the northern Qaidam Basin, northwest China. Chemie der Erde-Geochemistry 72, 245–252.
Clarkson, C.R., Jensen, J.L., Pedersen, P.K., Freeman, M., 2012. Innovative methods for flow-unit and pore-structure analyses in a tight siltstone and shale gas reservoir. AAPG Bull. 96, 355–374.
Coffey, B.P., Read, J.F., 2004. Mixed carbonate–siliciclastic sequence stratigraphy of a Paleogene transition zone continental shelf, southeastern USA. Sediment. Geol. 166, 21–57.
Curry, D.J., Emmett, J.K., Hunt, J.W., 1994. Geochemistry of aliphatic-rich coals in the Cooper Basin, Australia and Taranaki Basin, New Zealand: implications for the occurrence of potentially oil-generative coals. Geo. Soc. London Special Pub. 77, 149–181.
Damsté, J.S.S., Kenig, F., Koopmans, M.P., Köster, J., Schouten, S., Hayes, J.M., de Leeuw, J.W., 1995. Evidence for gammacerane as an indicator of water column stratification. Geochem. Cosmochim. Acta 59, 1895–1900.
Delpino, D.H., Bermúdez, A.M., 2009. Petroleum systems including unconventional reservoirs in intrusive igneous rocks (sills and laccoliths). Lead. Edge 28, 804–811.
De Castro, M.L., Priego-Capote, F., 2010. Soxhlet extraction: past and present panacea. J. Chromatogr. A 1217, 2383–2389.
Duan, Y., Zheng, C., Wang, Z., Wu, B., Wang, C., Zhang, H., Qian, Y., Zheng, G., 2006. Biomarker geochemistry of crude oils from the Qaidam Basin, NW China. J. Petrol. Geol. 29, 175–188.
Faill, R.T., 1969. Kink band structures in the Valley and Ridge province, central Pennsylvania. Geol. Soc. Am. Bull. 80, 2539–2550.
Farrimond, P., Taylor, A., Telnæs, N., 1998. Biomarker maturity parameters: the role of generation and thermal degradation. Org. Geochem. 29, 1181–1197.
Feng, J., Cao, J., Hu, K., Peng, X., Chen, Y., Wang, Y., Wang, M., 2013. Dissolution and its impacts on reservoir formation in moderately to deeply buried strata of mixed siliciclastic–carbonate sediments, northwestern Qaidam Basin, northwest China. Mar. Petrol. Geol. 39, 124–137.
Feng, J.L., Cao, J., Hu, K., Chen, Y., Yang, S.Y., Liu, Y.T., Bian, L.Z., Zhang, G.Q., 2011. Forming mechanism of middle-deep mixed rock reservoir in the Qaidam basin. Acta Petrol. Sin. 27, 2461–2472 (in Chinese with English abstract).
Fu, J., Sheng, G., Xu, J., Jia, R., Fan, S., Peng, P.A., Eglinton, G., Gowar, A.P., 1992. Biomarker compounds as indicators of paleoenvironments. Chin. J. Geochem. 11,

1–12.
Fu, S.T., 2010. Key controlling factors of oil and gas accumulation in the western Qaidam Basin and its implications for favorable exploration direction. Acta Sedimentol. Sin. 28, 373–379 (in Chinese with English abstract).
Fu, S., Ma, D., Chen, Y., Zhang, G., Wu, K., 2016. New advance of petroleum and gas exploration in Qaidam basin. Acta Pet. Sin. 37 (S1), 1–10 (In Chinese with English Abstract).
Garcia-Garcia, F., Soria, J.M., Viseras, C., Fernandez, J., 2009. High-frequency rhythmicity in a mixed siliciclastic–carbonate shelf (Late Miocene, Guadix Basin, Spain): a model of interplay between climatic oscillations, subsidence, and sediment dispersal. J. Sediment. Res. 79, 302–315.
Guan, P., Jian, X., 2013. The Cenozoic sedimentary record in Qaidam basin and its implications for tectonic evolution of the northern Tibetan plateau. Acta Sedimentol. Sin. 31, 824–833 (In Chinese with English Abstract).
Hanson, A.D., Ritts, B.D., Zinniker, D., Moldowan, J.M., Biffi, U., 2001. Upper Oligocene lacustrine source rocks and petroleum systems of the northern Qaidam basin, northwest China. AAPG Bull. 85, 601–620.
He, G., Tan, Y., Guan, P., Li, Y., Zhang, W., Du, B., 2008. Research on Tertiary oil source in the northwest Qaidam basin. Natural Gas Geosci 19, 509–518 (in Chinese with English abstract).
Huang, D., Zhang, D., Li, J., Huang, X., Zhou, Z., 1989. The Tertiary oil source correlation in Qaidam basin. Acta Sedimentol. Sin. 7, 1–13 (in Chinese with English abstract).
Hughes, W.B., Holba, A.G., Dzou, L.I., 1995. The ratios of dibenzothiophene to phenanthrene and pristane to phytane as indicators of depositional environment and lithology of petroleum source rocks. Geochem. Cosmochim. Acta 59, 3581–3598.
Ji, Y., Ma, D., Xue, J., Wang, P., Wu, Y., Zeng, L., Jin, L., 2017. Sedimentary environments and sedimentary model of carbonate rocks in the Cenozoic lacustrine basin, western Qaidam Basin. J. Palaeogeogr. 19, 757–772 (in Chinese with English abstract).
Jian, X., Guan, P., Fu, S.T., Zhang, D.W., Zhang, W., Zhang, Y.S., 2014. Miocene sedimentary environment and climate change in the northwestern Qaidam basin, northeastern Tibetan Plateau: facies, biomarker and stable isotopic evidences. Palaeogeogr. Palaeoclimatol. Palaeoecol. 414, 320–331.
Jian, X., Guan, P., Zhang, D.W., Zhang, W., Feng, F., Liu, R.J., Lin, S.D., 2013b. Provenance of Tertiary sandstone in the northern Qaidam basin, northeastern Tibetan Plateau: integration of framework petrography, heavy mineral analysis and mineral chemistry. Sediment. Geol. 290, 109–125.
Jian, X., Guan, P., Zhang, W., Feng, F., 2013a. Geochemistry of Mesozoic and Cenozoic sediments in the northern Qaidam basin, northeastern Tibetan Plateau: implications for provenance and weathering. Chem. Geol. 360, 74–88.
Jian, X., Guan, P., Zhang, W., Liang, H., Feng, F., Fu, L., 2018. Late Cretaceous to early Eocene deformation in the northern Tibetan Plateau: detrital apatite fission track evidence from northern Qaidam basin. Gondwana Res. 60, 94–104.
Jiang, X., Lu, Z., Sun, B., Liu, C., Fang, L., 2009. Evaluation of hydrocarbon source rocks in Xiaoliangshan sag, western Qaidam basin. Natural Gas Geosci 20, 405–410 (in Chinese with English Abstract).
Lee, H.S., Chough, S.K., 2011. Depositional processes of the Zhushadong and Mantou formations (Early to Middle Cambrian), Shandong Province, China: roles of archipelago and mixed carbonate–siliciclastic sedimentation on cycle genesis during initial flooding of the North China Platform. Sedimentology 58, 1530–1572.
Lu, J., Chen, S., Zhang, D., Fan, X., Wang, M., 2008. Hydrocarbon source and the accumulation in Jianding mountain, northwestern Qaidam basin. J. Southwest Petrol. Univ. (Sci. Technol. Edition) 30, 35–38 (in Chinese with English abstract).
Luo, Q., George, S.C., Xu, Y., Zhong, N., 2016. Organic geochemical characteristics of the Mesoproterozoic Hongshuizhuang Formation from northern China: implications for thermal maturity and biological sources. Org. Geochem. 99, 23–37.
Luo, Q., Qu, Y., Chen, Q., Xiong, Z., 2017. Organic geochemistry and petrology of mudrocks from the upper carboniferous batamayineishan formation, wulungu area, junggar basin, China: implications for petroleum exploration. Energy Fuel. 31, 10628–10638.
Luo, Q., Gong, L., Qu, Y., Zhang, K., Zhang, G., Wang, S., 2018a. The tight oil potential of the Lucaogou Formation from the southern Junggar Basin, China. Fuel 234, 858–871.
Luo, Q., Zhong, N., Liu, Y., Qu, Y., Ma, L., 2018b. Organic geochemical characteristics and accumulation of the organic matter in the jurassic to cretaceous sediments of the saihantala sag, erlian basin, China. Mar. Petrol. Geol. 92, 855–867.
Macquaker, J.H., Taylor, K.G., Keller, M., Polya, D., 2014. Compositional controls on early diagenetic pathways in fine-grained sedimentary rocks: implications for predicting unconventional reservoir attributes of mudstones. AAPG Bull. 98, 587–603.
Meyers, P.A., Ishiwatari, R., 1993. Lacustrine organic geochemistry—an overview of indicators of organic matter sources and diagenesis in lake sediments. Org. Geochem. 20, 867–900.
Mo, W., Zheng, Y., Zhang, W., Guan, P., 2007. Analysis of the youquanzi oil-bearing structure in Qaidam basin. Oil Gas Geol. 28, 324–328 (in Chinese with English abstract).
Moldowan, J.M., Sundararaman, P., Schoell, M., 1986. Sensitivity of biomarker properties to depositional environment and/or source input in the Lower Toarcian of SW-Germany. Org. Geochem. 10, 915–926.
Palermo, D., Aigner, T., Geluk, M., Poeppelreiter, M., Pipping, K., 2008. Reservoir potential of a lacustrine mixed carbonate/siliciclastic gas reservoir: The lower triassic rogenstein in the Netherlands. J. Petrol. Geol. 31, 61–96.
Pang, X., Zhao, W., Su, A., Zhang, S., Li, M., Dang, Y., Xu, F., Zhou, R., Zhang, D., Xu, Z., Guan, Z., Chen, J., Li, S., 2005. Geochemistry and origin of the giant Quaternary shallow gas accumulations in the eastern Qaidam Basin, NW China. Org. Geochem. 36, 1636–1649.
Pang, X.Q., Li, Y.X., Jiang, Z.X., 2004. Key geological controls on migration and accumulation for hydrocarbons derived from mature source rocks in Qaidam Basin. J. Petrol. Sci. Eng. 41, 79–95.
Philp, R.T., Gilbert, T.D., 1986. Biomarker distributions in Australian oils predominantly derived from terrigenous source material. Org. Geochem. 10, 73–84.
Pitman, J.K., Fouch, T.D., Goldhaber, M.B., 1982. Depositional setting and diagenetic evolution of some Tertiary unconventional reservoir rocks, Uinta Basin, Utah. AAPG Bull. 66, 1581–1596.
Poppelreiter, M., Aigner, T., 2003. Unconventional pattern of reservoir facies distribution in epeiric successions: lessons from an outcrop analog (Lower Keuper, Germany). AAPG Bull. 87, 39–70.
Seifert, W.K., 1978. Steranes and terpanes in kerogen pyrolysis for correlation of oils and source rocks. Geochem. Cosmochim. Acta 42, 473–484.
Stephens, N.P., Carroll, A.R., 1999. Salinity stratification in the Permian Phosphoria sea; a proposed paleoceanographic model. Geology 27, 899–902.
Song, C., Hu, S., Han, W., Zhang, T., Fang, X., Gao, J., Wu, F., 2014. Middle Miocene to earliest Pliocene sedimentological and geochemical records of climate change in the western Qaidam basin on the NE Tibetan Plateau. Palaeogeogr. Palaeoclimatol. Palaeoecol. 395, 67–76.
Song, H., Yi, H., Fan, A., Ma, X., Sun, X., 2010. Petrology and sedimentary environments of lacustrine carbonate rocks in the Xichagou Section, western Qaidam Basin. Chin. Geol. 37, 117–126 (in Chinese with English abstract).
Suppe, J., Sàbat, F., Munoz, J.A., Poblet, J., Roca, E., Vergés, J., 1997. Bed-by-bed fold growth by kink-band migration: sant Llorenç de Morunys, eastern Pyrenees. J. Struct. Geol. 19, 443–461.
Sun, M., Meng, Q., Fang, X., Wang, G., Huang, X., Wang, Z., Xu, Y., 2009. Geochemical significance of the microbial function of saturation hydrocarbon of calcilutites from the sebei well 1 of Qaidam basin. Acta Sedimentol. Sin. 27, 186–190 (in Chinese with English abstract).
Tang, L., Zhang, X., Long, G., Xu, F., Wang, B., Han, H., Xu, L., Yang, M., Li, H., Wang, G., 2013. Pool features and hydrocarbon accumulation analysis of lacustrine carbonate rock: take Nanyishan reservoir in Qaidam basin as an Example. Natural Gas Geosci 24, 591–598 (in Chinese with English abstract).
van Graas, G.W., 1990. Biomarker maturity parameters for high maturities: calibration of the working range up to the oil/condensate threshold. Org. Geochem. 16, 1025–1032.
Wang, E., Xu, F.Y., Zhou, J.X., Wan, J., Burchfiel, B.C., 2006. Eastward migration of the Qaidam basin and its implications for Cenozoic evolution of the Altyn Tagh fault and associated river systems. Geol. Soc. Am. Bull. 118, 349–365.
Wang, L., Jian, X., Yang, S., Guan, P., 2012. An Integrated Evaluation of Well L101 in Xiaoliangshan Area, Northwestern Qaidam Basin. Internal report of Qinghai Oilfield Company, PetroChina, pp. 1–151 (in Chinese).
Wang, T., Yang, S., Duan, S., Chen, H., Liu, H., Cao, J., 2015. Multi-stage primary and secondary hydrocarbon migration and accumulation in lacustrine Jurassic petroleum systems in the northern Qaidam Basin, NW China. Mar. Petrol. Geol. 62, 90–101.
Xia, W., Zhang, N., Yuan, X., Fan, L., Zhang, B., 2001. Cenozoic Qaidam basin, China: a stronger tectonic inversed, extensional rifted basin. AAPG Bull. 85, 715–736.
Yin, A., Dang, Y.Q., Zhang, M., Chen, X.H., McRivette, M.W., 2008. Cenozoic tectonic evolution of the Qaidam basin and its surrounding regions (Part 3): structural geology, sedimentation, and regional tectonic reconstruction. Geol. Soc. Am. Bull. 120, 847–876.
Yin, A., Harrison, T.M., 2000. Geologic evolution of the Himalayan-Tibetan orogen. Annu. Rev. Earth Planet Sci. 28, 211–280.
Yu, C., Guan, P., Zou, C., Wei, H., Deng, K., Wang, P., Wu, Y., 2016. Formation conditions and distribution patterns of N1 tight oil in Zhahaquan Area, Qaidam Basin, China. Energy Explor. Exploit. 34, 339–359.
Zecchin, M., Catuneanu, O., 2017. High-resolution sequence stratigraphy of clastic shelves VI: mixed siliciclastic-carbonate systems. Mar. Petrol. Geol. 88, 712–723.
Zeng, L., Tang, X., Wang, T., Gong, L., 2012. The influence of fracture cements in tight Paleogene saline lacustrine carbonate reservoirs, western Qaidam Basin, northwest China. AAPG Bull. 96, 2003–2017.
Zhang, N., Ren, X., Wei, J., Kang, Y., Zhang, C., 2006. Rock types of mixosedimentite reservoirs and oil-gas distribution in Nanyishan of Qaidam basin. Acta Pet. Sin. 27, 42–46 (in Chinese with English abstract).
Zhao, D., Zhang, M., Zhang, D., Yang, Q., Zhao, X., Liu, G., Hao, X., 2007. Maturity of Tertiary oil-source in western Qaidam basin. Acta Sedimentol. Sin. 25, 319–324 (in Chinese with English abstract).
Zhao, F., 2015. Lacustrine algal limestone reservoir in western Qaidam Basin, China. Carbonate. Evaporite 30, 127–133.
Zheng, Y., Mo, W., Zhang, W., Guan, P., 2007. A new idea for petroleum exploration in Qaidam basin. Petrol. Explor. Dev. 34, 13–18 (in Chinese with English abstract).
Zhou, J., Xu, F., Wang, T., Cao, A., Yin, C., 2006. Cenozoic deformation history of the Qaidam basin, NW China: results from cross-section restoration and implications for qinghai–tibet plateau tectonics. Earth Planet Sci. Lett. 243, 195–210.
Zhu, Y., Weng, H., Su, A., Liang, D., Peng, D., 2005. Geochemical characteristics of Tertiary saline lacustrine oils in the Western Qaidam Basin, northwest China. Appl. Geochem. 20, 1875–1889.
Zhuang, G., Hourigan, J.K., Ritts, B.D., Kent-Corson, M.L., 2011. Cenozoic multiple-phase tectonic evolution of the northern Tibetan Plateau: constraints from sedimentary records from Qaidam basin, Hexi Corridor, and Subei basin, Northwest China. Am. J. Sci. 311, 116–152.
Zou, C.N., Yang, Z., Tao, S.Z., Yuan, X.J., Zhu, R.K., Hou, L.H., Wu, S.T., Sun, L., Zhang, G.S., Bai, B., Wang, L., Gao, X.H., Pang, Z.L., 2013. Continuous hydrocarbon accumulation over a large area as a distinguishing characteristic of unconventional petroleum: the Ordos Basin, North-Central China. Earth Sci. Rev. 126, 358–369.